Catalysis Science & Technology

Accepted Manuscript

ROYAL SOCIETY OF CHEMISTRY

www.rsc.org/catalysis

Catalysis Science & Technology

Catalysis Science & Technology

Dynamic Article Links ►

Cite this: DOI: 10.1039/c0xx00000x

ARTICLE TYPE

www.rsc.org/xxxxxx

Effect of CO-pretreatment on the CuO-V_2O_5/γ-Al_2O_3 catalyst for NO reduction by CO

Yan Xiong,[a,c] Xiaojiang Yao,[a] Changjin Tang,[a] Lei Zhang,[a] Yuan Cao,[a] Yu Deng,[b] Fei Gao,[b] Lin Dong*[a, b]

Received (in XXX, XXX) Xth XXXXXXXXX 20XX, Accepted Xth XXXXXXXXX 20XX

DOI: 10.1039/b000000x

Abstract: The influence of CO-pretreatment on the properties of CuO-V_2O_5/γ-Al_2O_3 catalysts was investigated in the reaction of NO reduction by CO. Catalytic performances results showed that pretreated CuO-V_2O_5/γ-Al_2O_3 exhibited extremely high activity and selectivity. For example, NO conversion can be remarkably enhanced from 13.8 % to 100.0 % for 03Cu01V catalyst. For the catalyst characterization, XRD results suggested that copper oxide and vanadium oxide were highly dispersed on the surface of γ-Al_2O_3 and TPR results gave evidence for the existence of Cu^{2+}-O-V^{5+} species. XPS, EPR results demonstrated that Cu^{2+} and V^{5+} were reduced to lower valence states ($Cu^{2+}\rightarrow Cu^{+}$, $V^{5+}\rightarrow V^{4+}$) by the CO-pretreatment, which was proved by in situ FT-IR to be beneficial to the adsorption of CO and dissociation of NO. In addition, the interaction between dispersed copper oxide and vanadium oxide species upon the γ-Al_2O_3 support before and after CO-pretreatment was tentatively discussed in the concept of SSOV (surface synergetic oxygen vacancy) which was proposed elsewhere. According to this concept, the dispersed Cu^{2+}-O-V^{5+} species could be reduced to Cu^{+}-□-V^{4+} (□ represents oxygen vacancy) by CO-pretreatment and it was considered to be the primary active species for the reaction. Based on the discussion of experiment results, a possible mechanism was proposed.

1. Introduction

As a result of fast-growing vehicle population in developing countries, mobile source emission has become a major contributor to urban air pollution. Nitrogen oxides (NO_x) in vehicle emissions are generally believed to be responsible for many environmental problems such as acid rain, greenhouse effect and photochemical smog. Among various *de*NO_x technologies, catalytic elimination of NO_x by CO is likely to be one of the most promising approaches to meet current requirement, because generation of NO_x is always accompanied by formation of CO in an internal combustion engine. In such a system, if a suitable catalyst is applied, NO_x and CO could be converted to toxic N_2 and CO_2 simultaneously via a redox pathway, and thus greatly alleviate the pollution problems caused by vehicle emissions. Supported noble-metals, such as Rh, Pt, and Pd, were found to be effective in catalyzing NO+CO reaction.[1,2] However, the scarcity and high cost of these precious metals significantly limited their applications.[3] Great efforts have been devoted by researchers to searching for inexpensive materials as alternatives for noble-metal catalysts. Recently, a great deal of research has been focused on the investigation of transition metal oxides. Especially, copper oxide has caused a great interest because of its excellent redox property and adsorption ability for gas molecules.[4,5]

It is known that when a vehicle is running, the operation condition of its engine is not always constant. According to the air-fuel ratio (AFR) in a vehicle engine, the combustion status can be classified into three categories such as rich-burn (AFR<14.6), stoichiometric-burn (AFR=14.6), and lean-burn (AFR>14.6). Exhaust gases generated under these three combustion conditions are quite different in terms of composition. For example, rich-burn and lean-burn combustion create reducing and oxidizing atmosphere in the exhaust gases, respectively.[6] Current research on catalysts for automotive emission control mainly concentrate on lean-burn and stoichiometric conditions, and much less attention is paid to rich-burn combustion. A possible reason for this unbalanced research focus might be related to the fact that the reducing atmosphere generated by rich-burn combustion has negligible effect on the catalytic performance of noble-metal catalysts, since the active components of the catalysts are predominantly in reduced state. However, rich-burn combustion inevitably occurs during engine operation, especially at the cold-start stage. For transition metal oxide catalyst, the reductive exhaust gas has big impact on its existing status (valence state of transition metal and surface oxygen vacancies) of this type of catalyst are highly sensitive to reducing atmosphere. Thus, the atmospheric environment must be taken into consideration for investigation of transition metal

oxide catalysts. In this work, we simulated a reductive environment for the catalysis test of transition metal oxides by using CO-pretreatment. We believe that investigation on the changing nature of the structure, performance, and catalytic mechanism of transition metal oxide catalysts under reducing atmosphere could provide a more comprehensive framework for the development of efficient catalysts for automobile emission control.

In general, NO+CO reaction follows the redox-type mechanism that can be severely affected by the oxidation-reduction nature of reaction conditions.[7] This process usually involves the migration of oxygen species and formation of surface oxygen vacancies (SOV) in catalyst.[8] It has been proposed that SOV plays an important role in the reaction of NO removal, because it can act as the site for NO adsorption and dissociation.[9-11] For example, Wen *et al.* found that the excellent performance of $CuCeMgAlO_x$ catalyst was related to the formation of large amounts of SOV and Cu^+ ions reduced from Cu^{2+}.[12] SOV is generally expected to be formed readily under reducing atmosphere.[13] Jiang *et al.*, for instance, used reducing atmosphere pretreatment to investigate CuO/TiO_2 catalyst in NO+CO reaction.[8] In addition, Zhu[14] and his co-workers found a significant activity enhancement of $BiPO_{4-x}$ catalyst after de-oxidation treatment, and it was attributed to the formation SOV. In their work, activity of catalysts was proved to be dependent on the concentration and type of SOV, which could be controlled by tuning reduction temperature and time. However, the effect of reducing atmosphere on bi-component supported catalyst and its performance in NO+CO reaction are still not well understood. More research on this issue is required to clarify the reaction process so as to develop more effective catalysts for NO_x elimination.

The purpose of the present work is to assess the effect of CO-pretreatment on the properties and *de*NO_x performance of the catalysts in simulated rich-burn exhaust. After that, we wish to gain deeper insight into the structure-performance relationship of the catalysts in NO+CO reaction. Vanadium has been widely used as active component for NO elimination in NH_3-SCR. Furthermore, binary vanadium copper mixture on activated carbon was reported by Carabineiro *et al*. to exhibit synergetic effects in the NO reduction.[15] And the reduction of the vanadium and copper metal oxide was shown to be a key factor that controls the reaction. Therefore, copper and vanadium were chosen in this work to study the CO-pretreatment on the binary catalyst in NO+CO reaction. Supported binary metal oxide catalysts (CuO-V_2O_5/γ-Al_2O_3) were prepared by co-impregnation method and catalytic activities of the un-pretreated or CO-pretreated catalysts for the reduction of NO by CO were measured. Several techniques were used to characterize the physicochemical properties of the samples. Particular attentions are paid to: (1) Investigating the influence of CO-pretreatment on the activity, dispersion, and reduction properties of CuO-V_2O_5/γ-Al_2O_3 catalysts. (2) Exploring the role of reduced species in the model reaction of NO reduction by CO. (3) Further studying the nature of surface oxygen vacancy in bimetallic supported catalysts and approaching the synergetic working mechanism.

2. Experimental

2.1. Catalyst preparation

The γ-Al_2O_3 used as support was purchased from Fushun Petrochemical Institute of China. It was calcined in flowing air at 750 °C for 7 h before use and its Brunauer-Emmett-Teller (BET) surface area was 135 $m^2 \cdot g^{-1}$. The CuO/γ-Al_2O_3 and V_2O_5/γ-Al_2O_3 catalyst were prepared by wet impregnating γ-Al_2O_3 with aqueous solution containing requisite amount of $Cu(NO_3)_2 \cdot 3H_2O$ or NH_4VO_3, respectively. The solutions were kept in vigorously stirring for 2 h and evaporated at 100 °C in oil bath to vaporize the water. The resulting materials were dried at 110 °C for 12 h and finally calcined at 500 °C in flowing air for 5 h. For simplicity, the samples are denoted as *x*Cu and *y*V respectively, *e.g.*, 03Cu stands for the catalyst with copper oxide loading amount of 0.3 mmol Cu^{2+}/100 m^2 γ-Al_2O_3. The CuO-V_2O_5/γ-Al_2O_3 catalysts were prepared by co-impregnation of γ-Al_2O_3 with aqueous solution containing necessary amounts of $Cu(NO_3)_2 \cdot 3H_2O$ and NH_4VO_3. The excess water was evaporated and the resulting powder was dried at 110 °C overnight, calcined in flowing air at 500 °C for 5 h. Similarly, the samples are denoted as *x*Cu*y*V in the following. For example, 03Cu01V corresponds to CuO-V_2O_5/γ-Al_2O_3 catalyst with Cu^{2+} and V^{5+} loading amounts of 0.3 and 0.1 mmol/100 m^2 γ-Al_2O_3 respectively. In addition, the mechanical mixture of CuO/γ-Al_2O_3 and V_2O_5/γ-Al_2O_3 was prepared with weight ratio of 1:1 (denote as 03Cu+01V) to make comparison with $03Cu01V/\gamma$-Al_2O_3.

2.2. Catalyst characterization

The BET surface area was obtained by N_2-physisorption at 77 K on a Micromeritics ASAP-2020 analyzer. Prior to each analysis, the catalyst was degassed under vacuum at 300 °C for 3 h. Powder X-ray diffraction (XRD) patterns were recorded on a Philips X'pert Pro diffraction using Ni-filtered Cu Kα radiation (λ = 0.15418 nm). The X-ray tube was operated at 40 kV and 40 mA and the intensity data were collected over a 2θ range of 10—80°. The scan speed was set at 10° min^{-1} with a step size of 0.02°. H_2-temperature programmed reduction (H_2-TPR) experiments were performed in a quartz U-type reactor with Ar-H_2 mixture (7.0 % of H_2 by volume, 70 $mL \cdot min^{-1}$) as a reductant. The consumption of hydrogen was measured with a thermal conductivity detector (TCD). The sample (50 mg) was firstly pretreated in a high purified N_2 stream at 200 ºC for 1 h and cooled to room temperature. After that, the TPR started from 50 ºC to target temperature at heating rate of 10 $ºC \cdot min^{-1}$. X-ray photoelectron spectroscopy (XPS) analysis was performed on a PHI 5000 VersaProbe system, using monochromatic Al Kα radiation (1486.6 eV) operating at an accelerating power of 15 kW. Before the measurement, the sample was outgassed at room temperature in a UHV chamber (< 5×10^{-7} Pa). The sample charging effects were compensated by calibrating all binding energies (BE) with the adventitious C 1s peak at 284.6 eV. This reference gave BE values with accuracy at ±0.1 eV. Electron paramagnetic resonance (EPR) spectra were recorded on a Bruker EMX spectrometer using 100-kHz modulation and 4-G standard modulation width. The spectra were recorded at room temperature. For CO-pretreated sample, prior to testing, it was treated by flowing CO at 300 °C in a quartz tube and sealed into a glass tube under the protection of N_2. *In situ* Fourier transform infrared (*in situ* FT-IR) spectra of CO or/and NO adsorbed on the

catalyst were recorded on a Nicolet 5700 FT-IR spectrometer equipped with a DTGS as detector working at a spectral resolution of 4 cm^{-1} with scans number of 32 for each spectrum. The cell included a heating element and thermocouple, which provides feedback to a temperature controller in order to maintain a constant temperature at a set value. About 15 mg samples was pressed into a self-supporting wafer, and pretreated with high purified N_2 at 300 ºC for 1 h to remove impurities. After cooling to ambient temperature, gas flow of 10 % CO (balance Ar) or/and 5 % NO (balance Ar) was introduced into the IR cell for 30 min at a rate of 5.0 $mL \cdot min^{-1}$. CO or/and NO adsorption *in situ* FT-IR spectra were collected at various target temperatures at a rate of 10 $ºC \cdot min^{-1}$ from room temperature to 300 ºC by subtraction of the corresponding background reference.

2.3. Catalytic performances tests

The catalytic activity tests for the reduction of NO by CO were performed in a flow micro-reactor with reducing mixture of NO (5 %) and CO (10 %) balanced by He (85 %). A quartz tube with 25 mg catalyst (The catalyst powder was pressed and sieved through 18~32 mesh screen before used.) was pretreated in N_2 stream at 300 ^oC for 1 h and cooled to room temperature. After that, the gas reactants were switched on. The reaction was carried out along with the temperature increasing from 25 ^oC to 400 ^oC with a space velocity of 24, 000 $mL \cdot g^{-1} \cdot h^{-1}$. Two columns and thermal conduction detectors were used to analyze the products. Column A was packed with Paropak Q for separating N_2O and CO_2 and column B was packed with 5A and 13X molecular sieves (40—60 mesh) for separating N_2, NO and CO. The NO conversion and N_2 selectivity as used herein are defined from the concentrations of the inlet and outlet gases as follows:

$$\text{NO Conversion}\ (\%) = \frac{2([N_2]_{out} + [N_2O]_{out})}{[NO]_{in}} \times 100\%$$

$$N_2\ \text{Selectivity}\ (\%) = \frac{[N_2]_{out}}{[N_2]_{out} + [N_2O]_{out}} \times 100\%$$

In the case of CO-pretreatment, the samples were purged by N_2 at 300 ^oC, and then exposed to CO (10 % in He) for 1 h. The CO-pretreated samples were cooled to room temperature in flowing N_2 before the inletting of reaction gas. Being around the light-off temperature of fresh catalysts, 300 ^oC was chosen as the CO-pretreatment temperature in this measurement. The un-pretreated samples and CO-pretreated samples are labeled as *x*Cu*y*V(UP) and *x*Cu*y*V(CO), respectively.

3. Results and discussion

3.1. Catalytic performance results

Figure 1(a, b) shows the NO conversion and N_2 selectivity of catalysts with different loading amounts as a function of temperature. Both of the NO conversion and N_2 selectivity increase with the rising of reaction temperature. It can be readily observed that CO-pretreatment significantly improves the catalytic activities of some catalysts with the reaction temperature increment. It is noteworthy that the influence of CO-pretreatment on different catalysts is quite different. The significant enhancement of the catalytic activity for 03Cu01V caused by CO-pretreatment attracted our attention. Hence, mechanical mixture of 03Cu and 01V was adopted to make the problem more clear (denote as 03Cu+01V). The NO conversion and N_2 selectivity at 350 ^oC of the representative catalyst (03Cu, 01V, 03Cu01V and 03Cu+01V) is shown in Figure 1(c, d). It is obvious that 01V catalyst has little NO conversion at 350 ^oC before or after CO-pretreatment. The NO conversions of 03Cu and mechanical mixture are increased by 15 % and 5 % respectively after CO-pretreatment. For 03Cu01V, NO conversion can be remarkably enhanced from 13.8 % to 100.0 %, which is the greatest increasement under the same condition. We found that the effect of CO-pretreatment is not the same for samples with different vanadium loading amount. For example, different from other samples, 03Cu06V and 03Cu09V didn't show any increase of activity by CO-pretreatment at 300 ºC. The N_2 selectivity has similar trend with the NO conversion. This noticeable change possibly originates from different surface structures of the catalysts, which is further investigated by various characterization techniques in the following. Focusing on the supported bimetallic catalyst and mechanical mixture of single-metal catalysts, the crucial difference is probably that bimetallic catalyst has Cu-O-V species which is absent in the mechanical mixture. In the following chapters, 01V, 03Cu, 03Cu01V and 03Cu+01V are chosen as the main research objects to investigate the relationships between $deNO_x$ activities and the composition or structure of the catalyst.

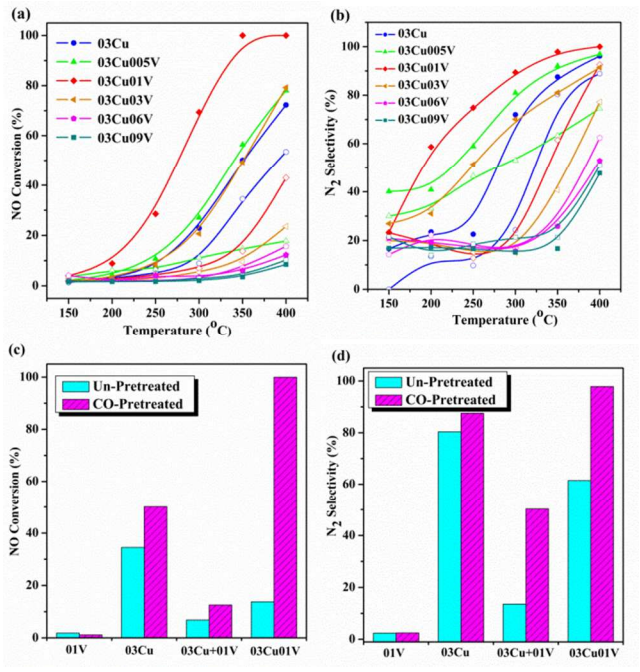

Figure 1 NO conversion and N_2 selectivity of the catalysts as a function of reaction temperature (a, b: hollow and solid symbols stand for un-pretreated and CO-pretreated samples, respectively) and some of the catalysts at 350 ^oC (c, d: 01V, 03Cu, 03Cu+01V and 03Cu01V)

3.2. XRD and XPS results

Powder XRD measurement of the catalysts was carried out to confirm the dispersed state of CuO and V_2O_5 on γ-Al_2O_3. XRD patterns of the un-pretreated samples and some pretreated

samples are shown in Figure 2a, b. No other diffraction peak except those for γ-Al_2O_3 support appears for the fresh samples (Figure 2a), indicating that copper oxide and vanadium oxide are highly dispersed on the surface of γ-Al_2O_3.[16] According to the literatures,[17,18] vanadium and copper in un-pretreated samples dispersed on the surface of the support and existed in the forms of V^{5+} and Cu^{2+}. In Figure 2b, signals at 43.3 and 50.4° in 03Cu(CO) are corresponding to characteristic peaks of crystalline metallic Cu^0 [JCPDS-04-0836]. By the comparison of the profiles, the typical diffraction signals of crystalline metal Cu^0 are almost invisible in 03Cu01V(CO) but more intense in 03Cu(CO). It declares that Cu^0 species in 03Cu01V(CO) is very few or the particle size is below the detection limit of XRD. This is probably ascribed to the interaction of Cu and V in 03Cu01V which inhibits the complete reduction of copper. No signal associate with crystalline vanadium species is detected in CO-pretreated samples, which suggests that vanadium is still well dispersed on the γ-Al_2O_3 support.

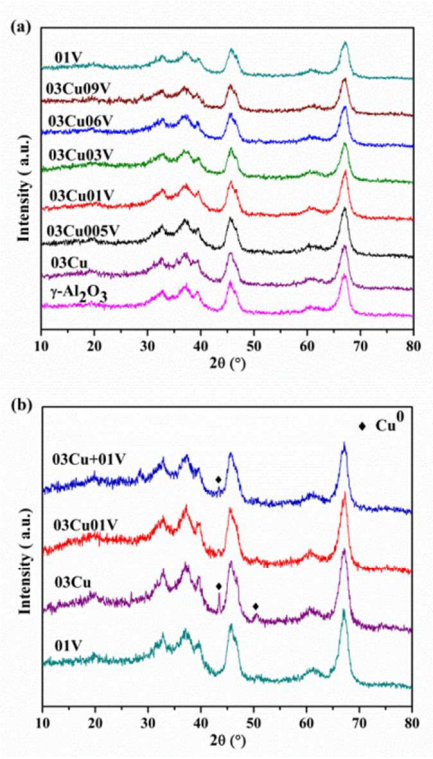

Figure 2 XRD patterns of (a) un-pretreated catalysts of different loadings and (b) samples after CO-pretreatment at 300 ºC (01V, 03Cu, 03Cu01V and 03Cu+01V)

XPS analysis was employed to confirm the valence and dispersion state of vanadium oxide and copper oxide species supported on γ-Al_2O_3. The Cu $2p_{3/2}$ and V $2p_{3/2}$ of the catalysts are display in Figure 3, and the overlapped peaks are fitted by Gaussian-Lorentz curves. A criterion of that one can estimate whether the signals attribute to Cu^{2+} or Cu^+/Cu^0 is the ratio between the intensities of the Cu $2p_{3/2}$ signal and its satellite at higher energies.[19] As shown in Figure 3(a–c) for Cu 2p spectra of the un-pretreated samples, 934.1 eV with satellite peak at 942.4 eV which is characteristic peaks of Cu^{2+} ions ($2p_{3/2}$). This indicates that oxidation state of copper in fresh sample is Cu^{2+}.[20] After CO-pretreatment, the satellite peaks virtually disappear and the peaks of Cu $2p_{3/2}$ transform to 932.7 eV which correspond to low-valence copper species (Cu^+ or/and Cu^0).[21] Moreover, when the spectra of Figure 3(a–c) are compared under the same ordinate scale, peak areas of Cu^{2+} and Cu^+/Cu^0 are found to be different. The area under the XPS curve is a measure of the Cu^+/Cu^0 concentrations, and thus the ratio of areas represents the variation in the relative concentrations of Cu species in the catalysts. So, peak area ratios of the Cu^{2+} (934.1 eV) or Cu^+/Cu^0 (932.7 eV) to Al 2p (74.4 eV) are evaluated and list in Table 1 in order to consider the surface dispersion distinction of copper on the support. For un-pretreated samples, this Cu^{2+}/Al ratio in CuV catalyst is larger than those in Cu catalyst and mechanic mixture, which implies that surface dispersion of copper in CuV sample is better than Cu sample. After CO-pretreatment, Cu^+(or Cu^0)/Al ratio in CuV catalyst is almost double of the ratio in Cu catalyst which evidences that the dispersity of low valence copper species become higher in CuV catalyst. This better surface dispersion of CuV catalyst is probably due to the interaction of Cu and V in binary metal catalyst. In other words, addition of vanadium is likely to result in an enrichment of surface copper of the catalyst which is positive correlation with the catalytic activity. This result is consistent with the conclusion that addition of V is beneficial to enhancing the dispersion of supported CuO species, which is responsible for the catalytic performance improving of Cu-based catalyst.[22] The enhancement of metal oxide phase dispersion on the support by addition of another component had also been reported by Nag *et al.*[23] and Bugyi *et al.*[24] Unfortunately, Cu $_{LMM}$ is difficult to distinguish Cu^+ and Cu^0 here for the low loading amount of Cu.

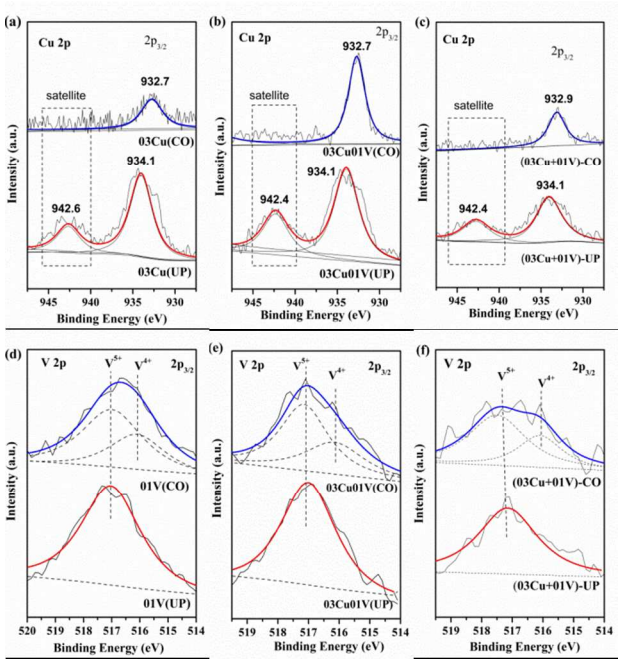

Figure 3 XPS spectra of Cu 2p for (a) 03Cu, (b) 03Cu01V, (c) 03Cu+01V and V 2p for (d) 01V, (e) 03Cu01V, (f) 03Cu+01V before and after CO-pretreatment

Table 1 XPS peak area ratio I_{Cu}/I_{Al} [between the Cu^{2+} (934.1 eV) or Cu^{+}, Cu^{0} (932.7 eV) and Al (74.4 eV)] of 03Cu, 03Cu01V, 03Cu+01V catalysts

Sample	I_{Cu}^{2+}/I_{Al}	Sample	$I_{Cu}^{+,Cu}{}^{0}/I_{Al}$
03Cu(UP)	30.93%	03Cu(CO)	13.71%
03Cu01V(UP)	43.82%	03Cu01V(CO)	24.22%
(03Cu+01V)-UP	21.05%	(03Cu+01V)-CO	11.34%

With regard to the valence change of vanadium species (Figure 3 d–f), it is obvious that only V^{5+} (517.1 eV) is the mainly present in un-pretreated catalysts. And that, V^{5+} (517.1 eV) and V^{4+} (516.1 eV) are co-existed in the pretreated samples.[25] It has been reported that when V^{4+} and V^{5+} exist together, unsaturated valence of V could promote the adsorption of oxygen and form reactive oxygen, which accelerate the process of NO_x reduction and increase the denitration activity.[26] All of the above features of surface analysis demonstrate the presence of $Cu^{2+}\rightarrow Cu^{+}/Cu^{0}$ and $V^{5+}\rightarrow V^{4+}$ during the CO-pretreatment process with an enrichment of surface copper in CuV catalysts. Combining with catalytic activities, it could be reasonable to infer that higher activity of CO-pretreated CuV sample than un-pretreated one is relevant to the reduced surface species and better dispersion.

3.3. Reduction behavior of catalysts (H_2-TPR results)

H_2-temperature programmed reduction (H_2-TPR) was performed to investigate the reducibility of the catalysts. Figure 4a is the H_2-TPR profile of 03Cu*y*V catalysts with different vanadium loading amounts and Figure 4b shows the fitted profiles of 03Cu, 01V, 03Cu01V, 03Cu+01V samples. For 01V, only a broad peak ranging from 300 °C to 550 °C can be observed in the profile which could be assigned to the reduction of V^{5+} ions on the surface of γ-Al_2O_3 support.[25] The areas of vanadium reduction peak in *y*V monometallic supported catalysts increase with the rising of V loading amounts and the reduction temperature scales are still 300~550 °C (not listed in Figure 4 for simplicity). For TPR profiles of CuV binary metal oxides samples, a multiple-step reduction is observed. Peak areas of H_2 consumption are calculated for *x*Cu*y*V catalysts and display in Table S1. It is found that *x*Cu*y*V samples can be reduced more easily than V sample and the location of the reduction temperatures depend on the loading amount of V. In addition, the area of reduction peak is always enhancing and reduction temperature shift to higher temperature with the increasing of vanadium loading amount. Similar H_2-TPR results of CuV catalyst had been reported by Zhang *et al*.[22]

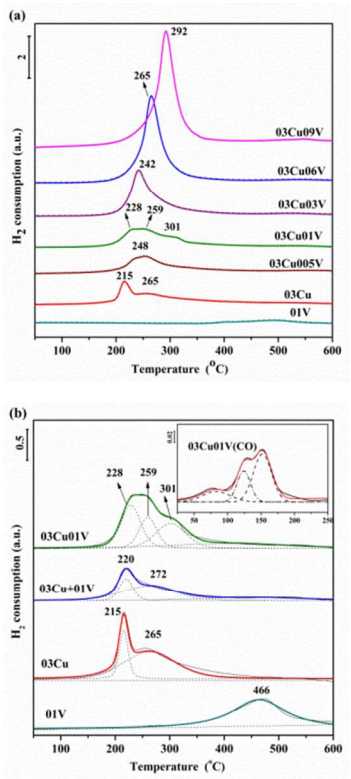

Figure 4 H_2-TPR profiles of *x*Cu*y*V catalysts (a) and fitted curves of 01V, 03Cu, 03Cu01V, 03Cu+01V (b)

It is a well-known that peak position and shape of H_2-TPR profile are highly sensitive to the nature of the catalyst. So, curve fitting was employed by Gaussian curves to get insight into the surface species of 03Cu, 03Cu01V, 03Cu+01V catalysts (Figure 4b). The inserted figure in Figure 4b is the H_2-TPR of the CO-pretreated 03Cu01V. The presence of more than one reduction peak in the bimetallic samples is an indication of the existence of several oxide species in the system. In the case of 03Cu, a much stronger peak with a maxima at 215 °C and a shoulder peak at 265 °C are observed, which represent the reduction of dispersed copper oxide. This is consistent with our previous work that Cu^{2+} on the surface of γ-Al_2O_3 with different coordination states could induce the appearance of this shoulder peak.[18] Similar results have been obtained by Venkov *et al*.[27] For the mechanical mixture, H_2-TPR profile looks like the superposition of two curves of 03Cu and 01V as you can see from Figure 4b. The H_2-TPR profile of 03Cu01V is different with the mechanical mixture that there were obviously four peaks. The peak at 259 °C with a shoulder peak at 301 °C was reduction peak of Cu^{2+} species and the broad peak at around 450 °C is assign to the reduction of V_2O_5. Furthermore, a new peak centered at 228 °C in 03Cu01V which is not appeared in Cu catalyst and mechanical mixture can be assigned to the reduction of Cu^{2+}-O-V^{5+} species (species consisting of Cu^{2+} and V^{5+} ions bridged by oxygen). It is worth noting that this peak was almost disappeared in the H_2-TPR of 03Cu01V(CO) sample (inserted figure in Figure 4b). Our explanation is that the easily reducible surface Cu^{2+}-O-V^{5+} species is already reduced by CO with the bridge oxygen being taken away before H_2-TPR test. This reduction might play a key role in improving the reaction activity. There is likely a synergistic effect in copper and vanadium originated by the contact and well dispersion of the

different oxides in catalysts preparation. Indeed, this strong interaction between different oxides catalysts had been reported for copper-zinc chromite catalyst[28] and copper-cerium catalyst.[29]

3.4. Chemical states of the catalysts (EPR results)

In light of the above, it is necessary to confirm the valence of copper and vanadium on the catalysts surface. EPR (Electron Paramagnetic Resonance) is a sensitive technique for investigating the oxidation states, surfaces, bulk coordination and the physical form of a transition metal oxide. EPR technique has been extensively employed to study powder oxide catalytic system, particularly Cu and V oxide.[30] In order to study oxidation states and the existence of interaction effects in binary systems (CuV), EPR of some samples were measured. Fig. 5 is the EPR spectra of 03Cu, 01V and 03Cu01V before and after CO-pretreatment. The EPR spin Hamiltonian parameters of surface copper and vanadium species in these samples were calculated and reported in Table S2. In the spectrum of 03Cu (Figure 5a), a strong axially symmetric signal with g = 2.330 attributed to Cu^{2+} species is observed.[31] The intensity of this signal decreases greatly after CO-pretreatment, which reveals that Cu^{2+} species is almost reduced to low valence states which has no EPR signal response. As shown in the EPR spectrum of 01V (Figure 5b), difference in the shape of the two lines clearly reflects different status of V in the un-pretreated and CO-pretreated sample. As reported, V^{5+} (electronic configuration is $3d^0$) ion is EPR silent due to the absence of any unpaired electron, while V^{4+} ($3d^1$) ions are EPR sensitive because the ^{51}V nucleus has a large magnetic moment, giving rise to informative hyperfine structure (S = 1/2; I = 7/2).[32] For vanadium on γ-Al_2O_3 in the 01V sample, signal of paramagnetic vanadium (V^{4+}) is characterized by an eight line spectrum appeared after CO-pretreatment. As indicated in Figure 5b, vanadium in the fresh sample is almost all V^{5+} species with traces of V^{4+}. And signal of V^{4+} appears in 01V(CO) with a strong resonance line at $g_{//}$ = 1.911, $A_{//}$ = 155 G. For 03Cu01V (Figure 5c), the un-pretreated sample only has EPR signal of Cu^{2+} ($g_{//}$ = 2.334, $A_{//}$ = 156 G) which disappears after CO-pretreatment and no signals of V^{4+} are detected. Meanwhile, EPR signal of V^{4+} ($g_{//}$ = 1.904, $A_{//}$ = 168 G, $g_{\perp}$ = 2.009, $A_{\perp}$ = 54 G) emerge after the CO-pretreatment. The same results of valance change in V_2O_5/γ-Al_2O_3 reduced by CO were also reported by Davydov *et al*.[33] A sharp signal of the g-value (g = 2.003) appears in 01V(CO) and 03Cu01V(CO) samples. Based on the literature,[34] it is characteristic of paramagnetic materials containing superoxide ions O_2^- which may be resulting from the oxygen vacancy. As proved by previous studies, the coordinative environment of the paramagnetic ion could be obtained by comparing its spin Hamiltonian parameters. In this case, $g_{//}$ of V^{4+} species in 03Cu01V catalyst are smaller than that in 01V, and $A_{//}$ values are greater, which suggests that its dealing with a weaker $(V\text{-}O)^{2+}$ species rather than VO^{2+}.[35] The EPR results implies that Cu^{2+} and V^{5+} are reduced to lower valence states ($Cu^{2+}\rightarrow Cu^{+}/Cu^{0}$, $V^{5+}\rightarrow V^{4+}$) by the CO-pretreatment, which corroborate the aforementioned results. Meanwhile, the oxygen atoms between Cu and V are supposed to be taken away by CO to form Cu^{+}-□-V^{4+} species what are considered beneficial to the reaction. The symbol □ is on behalf of surface oxygen vacancy.

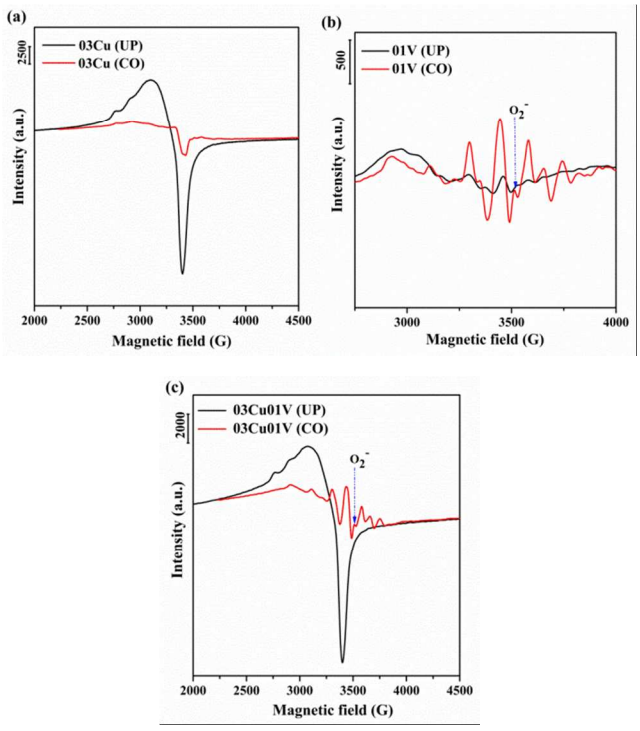

Figure 5 EPR spectra of (a) 03Cu, (b) 01V and (c) 03Cu01V samples. (Black line for un-pretreated samples and Red line for CO-pretreated samples)

3.5. CO or/and NO interaction with the catalysts (In situ FT-IR)

The *in situ* FT-IR of CO adsorption was carried out at various temperatures to understand the adsorption and reduction properties of these catalysts, and the corresponding results are present in Figure 6. Exposure of 01V sample to CO in the temperature regions between 25~300 ^{o}C does not bring any characteristic bands related to CO vibrations, so the spectra of 01V sample is not shown for brevity. It has been established that CO did not form vanadium carbonyls even at low temperatures, because of their high coordinative saturation and the covalent character of the V-O bond.[36] For 03Cu and 03Cu01V, the characteristic band associated with adsorbed CO molecules appears at about 2110 cm^{-1} at current operating conditions. It is generally acknowledged that carbonyl bands at wavenumbers about 2105–2150 cm^{-1} are due to carbonyl species adsorbed on Cu^{+} to form linear Cu^{+}-CO species.[37]

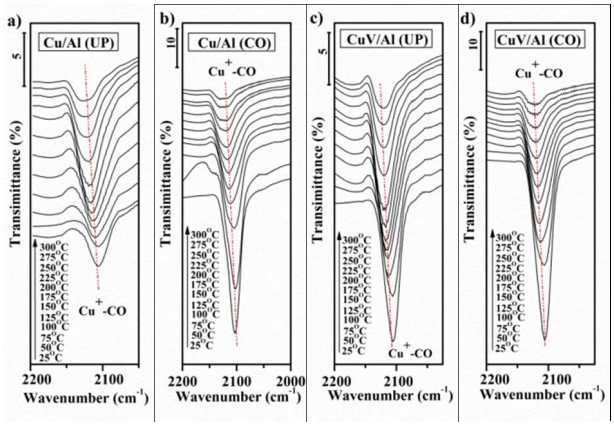

Figure 6 *In situ* FT-IR spectra of CO interaction with the catalysts from 25 ºC to 300 ºC at a heating rate of 10 ºC·min^{-1}

Appearance of Cu^+-CO peaks in the fresh samples at room temperature may be attributed to that N_2 purge at 300 ºC before collection could cause reduction of a small portion of Cu^{2+} to Cu^+. Indeed it is generally accepted that only Cu^+ can adsorb CO at room temperature while Cu^{2+}-CO and Cu^0-CO are not stable.[38] Previous literature showed that, Cu species on γ-Al_2O_3 is mainly reduced to Cu^+ by CO at 300 ºC and to large metal Cu^0 above 500 ºC.[39] As shown in Figure S1, there is no peak at 1900~2300 cm^{-1} for 03Cu01V sample purged in O_2 at 150 ºC. After pretreated by CO at 300 ºC, a strong peak at 2105 cm^{-1} appears which is attributed to Cu^+-CO. This peak vanished after 500 ºC CO-pretreatment because the copper are fully reduced to Cu^0. So, we can think from the IR spectra that Cu^{2+} were mostly reduced to Cu^+ by CO-pretreatment at 300 ºC. In regard to the intensity of Cu^+-CO in different samples, the evolution of Cu^+-CO species as a function of temperature are presented in Figure S2. The curves of 03Cu and 03Cu01V exhibit a similar trend. Firstly, the intensity of Cu^+-CO species increases with the temperature rising due to the reduction of Cu^{2+} to Cu^+. And then, it decreases with further temperature rising owing to the high-temperature desorption of CO. For the CO-pretreated samples, intensity of Cu^+-CO is on a declining curve because the copper is almost reduced to Cu^+ in the CO-pretreatment process. It is worth noting that the intensity of Cu^+-CO of CuV catalyst is always higher than that of Cu catalyst both in fresh and pretreated sample. This could be deduced that copper in CuV catalyst is easier to be reduced than that of Cu catalyst. And this is accordant with the catalytic performance results, considering Cu^+ is generally beneficial to the enhancement of catalytic activity in NO+CO reaction. We also notice that there is a small blue-shift of Cu^+-CO adsorption peak related to the enhancement of ν(C-O) vibration strength in all the samples. This is perhaps due to the decrease of adsorption capability between CO and solid surface caused by the intensification of thermal motion during temperature rising. In other words, the interaction of CO with the catalysts is weakened by the temperature increasing, thus the C-O bond is strengthened.[40]

In situ FT-IR for NO and CO co-interaction with un-pretreated and CO-pretreated catalysts were performed to further clarify the surface reaction of NO reduction by CO during the heating process. As shown in Figure 7, series of bands are observed in the 1000–1800 cm^{-1} region and 2000–2300 cm^{-1} region, which belongs to the nitrate/nitrite species and carbonate species. According to literatures,[27,41,42] bridging bidentate nitrate exhibits N=O stretching model at 1624–1629 cm^{-1}. Chelating bidentate nitrate shows two bands at 1219–1223 cm^{-1} and 1564 cm^{-1}. Linear nitrite has the NO_2 asymmetric vibration band at 1269–1273 cm^{-1}. Monodentate nitrate gives two bands at 1296–1300 cm^{-1} and 1488–1506 cm^{-1}. Bridging monodentate nitrate displays a band at 1560 cm^{-1}. With reference to the above results in the literatures, assignments of the adsorption peaks are demonstrated in the Figure 7. In the spectra, physical adsorbed NO species gives a band at 1745 cm^{-1} which only appears under 150 ºC due to its poor stability. With the rising temperature, the bands of the monodentate nitrate (1300, 1500 cm^{-1}), bridging bidentate nitrate (1624 cm^{-1}) show a decreasing tendency in intensity and disappear gradually. When the temperature is up to about 150 ºC, a new band (1550–1560 cm^{-1}) assigned to chelating bidentate nitrate appears, which indicate that the adsorbed NO species can be converted to chelated nitrate/nitrite species. The temperature rising practically leads to intensity decrease of the bands at 1624 cm^{-1} and 1560 cm^{-1} for bridging bidentate nitrate and chelating bidentate nitrate (the later not be completely disappeared till 300 ºC). It demonstrates that the chelated nitrate has better stability than the bridged bidentate nitrate. Based on the literatures,[33,43] FT-IR signals of NO adsorption on V^{5+} cation cannot be detected at ambient temperature, but V^{4+} produced from CO-pretreatment can adsorb NO to form V^{4+}-NO and V^{4+}-$(NO)_2$. So we hold the opinion that reduction of vanadium species by CO-pretreatment is one of the reasons of catalytic activity enhancement in CuV sample.

Concerning the spectral features in the region of 2000–2500 cm^{-1}, one can distinguish bands at 2103 cm^{-1}, 2142 cm^{-1}, 2207 cm^{-1} and 2242 cm^{-1}. On the basis and in agreement with previous studies,[44,45] we attribute the bands to Cu^+-CO (2103 cm^{-1}), Cu^+-$(CO)_2$ (2142 cm^{-1}), -NCO (2207 cm^{-1}), N_2O (2242 cm^{-1}) respectively. No band of Cu^+-CO is observed below 200 ºC in the spectra of CO+NO co-adsorption which is different with CO adsorption spectra. It is possibly because the competitive adsorption of NO and CO. CO interacted with Cu species in lower temperature is replaced by NO. In consideration of the reaction process, NCO and N_2O are known to be produced from the recombination of nitrate species and surface adsorbed CO. So, presence of the intermediate NCO and N_2O reflects the occurrence of NO+CO reaction on the catalyst surface. The intermediate NCO can only be detected above 200 ºC which fits with that the reaction shown obvious activities when the temperature reached 200 ºC. Comparison of the spectra of Figure 7(a–d) indicates that band of N_2O (2242 cm^{-1}) does not appear until 275 ºC in fresh samples while it is always exist in the pretreated samples. This is in agreement with the results of CO-pretreated samples have higher catalytic activity than fresh samples.

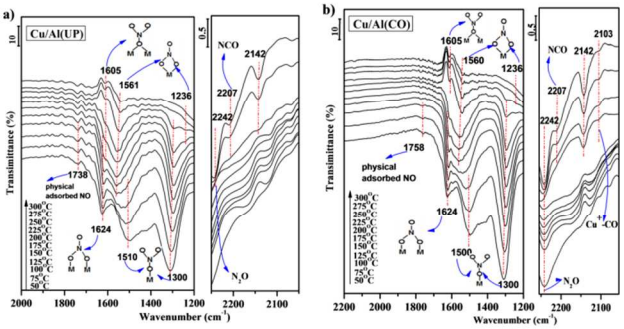

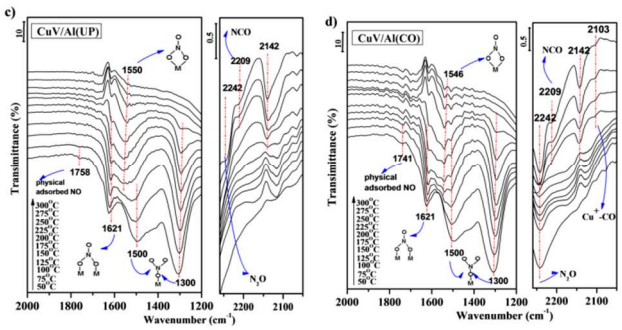

Figure 7 *In situ* FT-IR results of CO and NO co-interaction with the catalysts from 50 to 300 ºC at a heating rate of 10 ºC·min^{-1} (The models of adsorbed species were displayed in the figure)

3.6. Possible reaction mechanism

Based on the above results and discussion, a possible reaction mechanism is tentatively proposed as follows (Figure 8) to further understand the remarkable enhancement of the catalytic performance results from CO-pretreatment. According to the report,[46] the dissociation of NO is the key step for NO removal by CO and oxygen vacancy can activate the N-O bond to promote this dissociation. Surface oxygen vacancy has been reported to have a high reactivity toward N_2O dissociation by Chen *et al.*[47] In our case, CO-pretreatment on CuO-V_2O_5/γ-Al_2O_3 catalysts leads to the reduction of $Cu^{2+}\rightarrow Cu^{+}$ and $V^{5+}\rightarrow V^{4+}$. And Cu^{+} or V^{4+} is conducive to the adsorption and activation of CO or NO. Simultaneously, the CO-pretreatment actually reduces the catalyst surface by taking away the surface oxygen to generate more vacancies. It is above reasons that lead to the great activity promotion caused by the CO-pretreatment. When exposing the catalyst to CO and NO mixture gases, the CO molecules preferred to adsorb on Cu^{+} sites rather than V^{4+} sites. The CO species adsorbed on Cu^{+} can combine with O radicals come from the dissociation of NO_{ads} on the adjacent oxygen vacancy to form CO_2. The resulting N_{ads} is recombined with NO_{ads} or CO to give N_2O or NCO respectively, or their own combination to generate N_2. The by-product N_2O can further dissociate with the assistance of oxygen vacancy, thereby evolving into N_2 and O_{ads}. Then neighbouring CO combined with O_{ads} to form CO_2 and regenerated new active sites on the surface.

For CuO/γ-Al_2O_3 or V_2O_5/γ-Al_2O_3 samples, there is only Cu^{2+}-O-Cu^{2+} or V^{5+}-O-V^{5+} species on the surface. So the removal of O atom by CO from the surface of CuO/γ-Al_2O_3 or V_2O_5/γ-Al_2O_3 will result in Cu^{+}-□-Cu^{+} or V^{4+}-□-V^{4+} (surface oxygen vacancy, SOV). Formation of Cu^{+}-□-Cu^{+} species during CO-pretreatment is beneficial to the reaction due to it has active sites for the adsorption of CO and dissociation of NO. However, both the adjacent sites of oxygen vacancy are Cu^{+} in Cu^{+}-□-Cu^{+}. Therefore, adsorption of CO on neighbouring Cu^{+} can generate some steric effect for the adsorption and dissociation of NO on the oxygen vacancy. For V^{4+}-□-V^{4+} species, its promoting role in the reaction is not obvious, because that V^{4+} cannot provide the adsorption sites for CO molecules efficiently. With regard to CuO-V_2O_5/γ-Al_2O_3 catalysts, it may form three kinds of oxygen vacancies during the CO-pretreatment process: Cu^{+}-□-V^{4+} species, as well as Cu^{+}-□-Cu^{+} and V^{4+}-□-V^{4+}species. The vacancy in Cu^{+}-□-V^{4+} species is referred to surface synergetic oxygen vacancy (SSOV) for that it is assumed to have synergistic effect between oxygen vacancy and two adjacent different ions. In view of Cu^{+}-□-V^{4+} species, the adjacent sites of oxygen vacancy are Cu^{+} and V^{4+}, the steric effect for the dissociation of NO on oxygen vacancy would be smaller, because that V^{4+} does not adsorb CO. And that the bridge oxygen in Cu^{2+}-O-V^{5+} species is easier to be removed by CO to generate oxygen vacancy than oxygen in Cu^{2+}-O-Cu^{2+} or V^{5+}-O-V^{5+}. As a result, we believe that the surface synergetic oxygen vacancy (SSOV) can enhance the catalytic performance more effectively than surface oxygen vacancy (SOV). The SSOV can be only generated in bi-metal catalysts rather than single-metal sample or mechanical mixture of single-metal samples. This viewpoint can be used to explain the difference of promotion effect caused by CO-pretreatment between bi-metal and single-metal catalysts or the mechanical mixture. On the basis of above discussion, the SSOV was considered to play a critical role as a bridge in enhancing the reactive effectiveness. Similar results in CuO/MnO_x/γ-Al_2O_3 and CuO-CoO/γ-Al_2O_3 and $Ce_xSn_{1-x}O_2$ mixed oxide catalyst have also been found.[48-50] In this work, formation of SSOV in samples with different vanadium loadings are found to be different during CO-pretreatment. As far as 03Cu06V and 03Cu09V were concerned, catalytic performances can also increase significantly when the CO-pretreat temperature are high enough. For example, SSOV can be generated in 03Cu06V and 03Cu09V by 350 and 425 ºC CO-pretreatment which results in the promotion (Figure S3). As the evolution of our previous work, this study enlarges the universality of the SSOV and makes the research step forward.

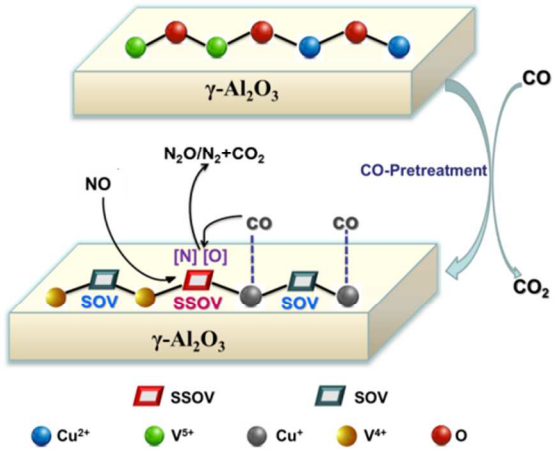

Figure 8 Schematic representation of the proposed mechanism for NO+CO reaction over CuO-V_2O_5/γ-Al_2O_3 catalyst

4. Conclusions

The CuO-V_2O_5/γ-Al_2O_3 catalysts were prepared via co-impregnation method and used for NO reduction by CO in a simulated reducing rich-burn exhaust. CO-pretreatment, as a reduction method, was used to explore the effect of reducing treatment on the properties and activity of catalysts. Samples pretreated by CO at 300 °C showed significantly higher catalytic activities than the un-pretreated samples. From the comparing study, increase of catalytic performance resulting from CO-pretreatment for CuO-V_2O_5/γ-Al_2O_3 is more significant than

that of single component supported catalysts or mechanical mixture of them. Results indicated that dispersed Cu^{2+}-O-V^{5+} species on the surface of CuO-V_2O_5/γ-Al_2O_3 was reduced to Cu^{+}-□-V^{4+} and the surface oxygen vacancy produced simultaneously. The surface oxygen vacancy in Cu^{+}-□-V^{4+} species is believed to be a bridge to contact the adjacent adsorbed species and facilitates the dissociation of adsorbed NO. And that it is regarded as the surface synergetic oxygen vacancy (SSOV) for the synergistic effect. Moreover, this SSOV (Cu^{+}-□-V^{4+}) is more favorable to the NO+CO reaction than SOV (Cu^{+}-□-Cu^{+}) due to its smaller steric effect. Herein, we consider the Cu^{+}-□-V^{4+} species as a catalytic domain which plays a key role in the catalytic reaction due to the synergistic effect between different adjacent ions (Cu^{+} and V^{4+}) and oxygen vacancy. Formation of the SSOV is used to explain why the promotion of activity caused by CO-pretreatment for bi-metal oxide catalysts is much greater than that for single-metal oxide catalysts or mechanical mixture. This work could probably provide inspirations for developing correlation between physicochemical properties and catalytic performances of the supported bi-metal oxide catalysts.

Acknowledgements

The financial supports of the National Natural Science Foundation of China (Nos. 21273110, 21303082), the National Basic Research Program of China (973 program, No. 2010CB732300), the Doctoral Fund of Ministry of Education of China (2013009111005) and Sinopec Shanghai Research Institute of Petrochemical Technology are gratefully acknowledged.

Notes and references

[a]*Key Laboratory of Mesoscopic Chemistry of MOE, School of Chemistry and Chemical Engineering, Nanjing University, Nanjing, 210093, P. R. China*
[b]*Jiangsu Key Laboratory of Vehicle Emissions Control, Center of Modern Analysis, Nanjing University, Nanjing 210093, PR China*
[c]*College of Chemistry and Pharmaceutical Engineering, Nanyang Normal University, Nanyang 473061, PR China*
Corresponding author:
Fax: +86 25 83317761; Phone: +86 25 83592290
Address: Hankou Road 22#, Nanjing, Jiangsu province, P. R. China, 210093
E-mail address: donglin@nju.edu.cn (L. Dong)

1 P. Bera, K. C. Patil, V. Jayaram, G. N. Subbanna, M. S. Hegde, *J. Catal.* **2000**, *196*, 293-301.
2 T. Chafik, D. I. Kondarides, X. E. Verykios, *J. Catal.* **2000**, *190*, 446-459.
3 V. I. Pârvulescu, P. Grange, B. Delmon, *Catal. Today* **1998**, *46*, 233-316.
4 Q. Yu, X. J. Yao, H. L. Zhang, F. Gao, L. Dong, *Appl. Catal. A: Gen.* **2012**, *423*, 42-51.
5 A. Patel, P. Shukla, T. Rufford, S. B. Wang, J. L. Chen, V. Rudolph, Z. H. Zhu, *Appl. Catal. A: Gen.* **2011**, *409*, 55-65.
6 W. Bögner, M. krämer, B. Krutzsch, S. Pischinger, D. Voigtländer, G. Wenninger, F. Wirbeleit, M. S. Brogan, R. J. Brisley, D. E. Webster, *Appl. Catal. B: Environ.* **1995**, *7*, 153-171.
7 M. Fernández-García, C. Márquez-Alvarez, I. Rodríguez-Ramos, A. Guerrero-Ruíz, G. L. Haller, *J. Phys. Chem.* **1995**, *99*, 16380-16382.
8 X. Y. Jiang, Y. R. Jia, P. H. Huan, X. M. Zheng, *Catal. Lett.* **2005**, *104*, 169-175.
9 J. D. A. Bellido, E. M. Assaf, *Fuel* **2009**, *88*, 1673-1679.
10 J. F. Chen, J. J. Zhu, C. Q. Chen, Y. Y. Zhan, Y. N. Cao, X. Y. Lin, Q. Zheng, *Catal. Lett.* **2009**, *130*, 254-260.
11 S. J. Huang, A. B. Walters, M. A. Vannice, *J. Catal.* **2000**, *192*, 29-47.
12 B. Wen, M. Y. He, *Appl. Catal. B: Environ.* **2002**, *37*, 75-82.
13 A. Martínez-Arias, J. Soria, J. C. Conesa, X. L. Seoane, A. Arcoya, R. J. Cataluña, *J. Chem. Soc.: Faraday Trans,* **1995**, *91*, 1679-1687.
14 X. J. Bai, L. Wang, R. L. Zong, Y. H. Lv, Y. Q. Sun, Y. F. Zhu, *Langmuir* **2013**, *29*, 3097-3105.
15 S. A. Carabineiro, F. B. Fernandes, J. S. Vital, A. M. Ramosa, I. M. Fonseca, *Appl. Catal. B: Environ.* **2003**, *44*, 227–235.
16 M. S. P. Francisco, V. R. Mastelaro, P. A. P. Nascente, A. O. Florentino, *J. Phys. Chem. B* **2001**, *105*, 10515-10522.
17 Z. L. Wu, P. C. Stair, S. Rugmini, S. D. Jackson, *J. Phys. Chem. C* **2007**, *111*, 16460-16469.
18 H. Q. Wan, Z. Wang, J. Zhu, X. W. Li, B. Liu, F. Gao, L. Dong, *Appl. Catal. B: Environ.* **2008**, *79*, 254-261.
19 J. Morales, A. Caballero, J. P. Holgado, J. P. Espinós, A. R. González-Elipe, *J. Phys. Chem. B* **2002**, *106*, 10185-10190.
20 M. Yin, C. K. Wu, Y. B. Lou, C. Burda, J. T. Koberstein, Y. M. Zhu, S. O'Brien, *J. Am. Chem. Soc.* **2005**, *127*, 9506-9511.
21 J. L. Gong, H. R. Yue, Y. J. Zhao, S. Zhao, L. Zhao, J. Lv, S. P. Wang, X. B. Ma, J. Am. Chem. Soc., **2012**, *134*, 13922-13925.
22 Y. P. Zhang, J. H. Fei, Y. M. Yu, X. M. Zheng, *J. Nat. Gas Chem.* **2007**, *16*, 12-15.
23 N. K. Nag, *J. Phys. Chem.* **1987**, *91*, 2324-2327.
24 L. Bugyi, A. Berko, L. Ovari, A. M. Kiss, J. Kiss, *Surf. Sci.* **2008**, *602*, 1650-1658.
25 M. E. Harlin, V. M. Niemi, A. O. I. Krause, *J. Catal.* **2000**, *195*, 67-78.
26 X. Tian, Y. Xiao, P. Zhou, W. Zhang, X. Luo, *Mater. Res. Innov.*, **2014**, *18*, 202-206.
27 T. Venkov, M. Dimitrov, K. Hadjiivanov, *J. Mol. Catal. A: Chem.* **2006**, *243*, 8-16.
28 G. Fierro, M. Lo Jacono, M. Inversi, P. Porta, F. Cioci, R. Lavecchia, *Appl. Catal. A: Gen.* **1996**, *137*, 327-348.
29 W. J. Shan, Z. C. Feng, Z. L. Li, J. Zhang, W. J. Shen, C. Li, *J. Catal.* **2004**, *228*, 206-217.
30 R. Cousin, S. Capelle, E. Abi-Aad, D. Courcot, A. Aboukaïs, *Chem. Mater.* **2001**, *13*, 3862-3870.
31 G. V. Sagar, P. V. R. Rao, C. S. Srikanth, K. V. R. Chary, *J. Phys. Chem. B* **2006**, *110*, 13881-13888.
32 D. Srinivas, W. F. Hoderich, S. Kujath, M. H. Valkenberg, T. Raja, L. Saikia, R. Hinzeb, V. Ramaswamy, *J. Catal.* **2008**, *259*, 165-173.
33 A. A. Davydov, *Russ. Chem. Bull.* **1994**, *43*, 214-218.
34 H.Y. Li, S. L. Zhang, Q. Zhong, *J. Colloid Interface Sci.* **2013**, *402*, 190-195.
35 K. V. R. Chary, B. M. Reddy, N. K. Nag, V. S. Subrahmanyam. *J. Phys. Chem.* **1984**, *88*, 2622-2624.
36 Z. Sobalik, R. Kozlowski, J. Haber, *J. Catal.* **1991**, *127*, 665-674.
37 H. Praliaud, S. Mikhailenko, Z. Chajar, M. Primet, *Appl. Catal. B: Environ.* **1998**, *16*, 359-374.
38 G. Spoto, A. Zecchina, S. Bordiga, G. Ricchiardi, G. Marta, G. Leofanti, G. Petrini, *Appl. Catal. B: Environ.* **1994**, *3*, 151-172.
39 A. Martinez-Arias, R. Cataluna, J. C. Conesa and J. Soria, *J. Phys. Chem. B,* **1998**, *102*, 809-817.
40 O. Dulaurent, X. Courtois, V. Perrichon, D. Bianchi, *J. Phys. Chem. B* **2000**, *104*, 6001-6011.
41 L. J. Liu, B. Liu, L. H. Dong, J. Zhu, H. Q. Wan, K. Q. Sun, B. Zhao, H. Y. Zhu, L. Dong, Y. Chen, *Appl. Catal. B: Environ.* **2009**, *90*, 578-586.
42 K. I. Hadjiivanov, *Catal. Rev.* **2000**, *42*, 71-144.
43 A. A. Davydov, *Kinet. Catal.* **1993,** *34*, 295-301.
44 R. D. Zhang, W. Y. Teoh, R. Amal, B. H. Chen, S. Kaliaguine, *J. Catal.* **2010**, *272*, 210-219.
45 D. Scarano, S. Bordiga, C. Lamberti, G. Spoto, G. Richiardi, A. Zecchina, C. O. Areán, *Surf. Sci.* **1998**, *411*, 272-285.
46 A. G. Makeev, N. V. Peskov, *Appl. Catal. B: Environ.* **2013**, *132*, 151-161.
47 W. K. Chen, B. Z. Sun, X. Wang, C. H. Lu, *J. Theor. Comput. Chem.* **2008**, *07*, 263-276.

48 D. Li, Q. Yu, S. S. Li, H. Q. Wan, L. Qi, B. Liu, F. Gao, L. Dong, ***Chem-Eur. J.*** **2011**, *17*, 5668-5679.
49 Y. Y. Lv, L. C. Liu, H. L. Zhang, X. J. Yao, F. Gao, K. A. Yao, L. Dong, Y. Chen, *J. Colloid Interface Sci.* **2013**, *390*, 158-169.
50 X. J. Yao, Y. Xiong, W. X. Zou, L. Zhang, S. G. Wu, X. Dong, F. Gao, Y. Deng, C. J. Tang, Z. Chen, L. Dong, Y. Chen, *Appl. Catal. B: Environ.* **2014**, *144*, 152-165.